

# The dynamics of brain and cerebrospinal fluid growth in normal versus hydrocephalic mice

## Laboratory investigation

JASON G. MANDELL, M.S.,<sup>1,2</sup> THOMAS NEUBERGER, PH.D.,<sup>3</sup> CORINA S. DRAPACA, PH.D.,<sup>1</sup>  
ANDREW G. WEBB, PH.D.,<sup>4</sup> AND STEVEN J. SCHIFF, M.D., PH.D.<sup>1,3,5</sup>

<sup>1</sup>Center for Neural Engineering, Department of Engineering Science and Mechanics, <sup>2</sup>Department of Bioengineering, <sup>3</sup>Huck Institutes of the Life Sciences, and <sup>5</sup>Departments of Neurosurgery and Physics, Pennsylvania State University, University Park, Pennsylvania; and <sup>4</sup>C. J. Gorter Center for High Field MR Imaging, Department of Radiology, Leiden University Medical Center, Leiden, The Netherlands

**Object.** Hydrocephalus has traditionally been quantified by linear measures of ventricular size, with adjunct use of cortical mantle thickness. However, clinical outcome depends on cognitive function, which is more directly related to brain volume than these previous measures. The authors sought to quantify the dynamics of brain and ventricular volume growth in normal compared with hydrocephalic mice.

**Methods.** Hydrocephalus was induced in 14-day-old C57BL/6 mice by percutaneous injection of kaolin into the cisterna magna. Nine hydrocephalic and 6 normal mice were serially imaged from age 2–12 weeks with a 14.1-T MR imaging unit. Total brain and ventricle volumes were calculated, and linear discriminant analysis was applied.

**Results.** Two very different patterns of response were seen in hydrocephalic mice compared with mice with normative growth. In one pattern (3 mice) brain growth was normal despite accumulation of CSF, and in the second pattern (6 mice) abnormal brain enlargement was accompanied by increased CSF volume along with parenchymal edema. In this latter pattern, spontaneous ventricular rupture led to normalization of brain volume, implying edema from transmantle pressure gradients. These 2 patterns of hydrocephalus were significantly discriminable using linear discriminant analysis ( $p < 0.01$ ). In contrast, clinically relevant measurements of head circumference or frontal and occipital horn ratios were unable to discriminate between these patterns.

**Conclusions.** This study is, to the authors' knowledge, the first serial quantification of the growth of brain and ventricle volumes in normal versus hydrocephalic development. The authors' findings demonstrate the feasibility of constructing normative curves of brain and fluid growth as complements to normative head circumference curves. By measuring brain volumes, distinct patterns of brain growth and enlargement can be observed, which are more likely linked to cognitive development and clinical outcome than fluid volumes alone. (DOI: 10.3171/2010.4.PEDS1014)

**KEY WORDS** • hydrocephalus • magnetic resonance imaging • kaolin • cerebrospinal fluid • cerebral ventricle • development • brain growth

**H**YDROCEPHALUS is a disorder resulting in the accumulation of intracranial CSF due to abnormal CSF production, circulation, or absorption.<sup>31</sup> Even with the rapid advancement of neuroimaging technology, shunt-valve design, and surgical techniques, outcomes in patients with hydrocephalus have changed very little in the past 50 years.<sup>10</sup> This lack of progress may be due to the fact that current treatment protocols, aimed at decreasing excess fluid in the intracranial cavity, have also changed little. The fluid diversionary shunt was the first effective treatment developed and is still the most widely used form of treatment today.<sup>18</sup>

It has been known since the first models of experimental hydrocephalus created by Dandy<sup>7</sup> that hydrocephalus

is accompanied by pathophysiological changes in brain morphology. Since then, studies have shown that hydrocephalus can result in a thinning of the cortex, as well as an increase in the water content and loss of myelin in the periventricular white matter.<sup>8,23,25</sup> Despite known morphological changes of brain tissue in the development of hydrocephalus, experimental work has focused on measurements of the ventricular system—mainly linear measurements of ventricular size alone<sup>7</sup> or ratios of ventricle to brain thickness and area.<sup>5,19,22,29,30</sup> When studies have included linear measurements of cortex on an imaging section, the authors have often not taken into account other areas of the brain or total brain volumes.<sup>4,17</sup> Head circumference mea-

This article contains some figures that are displayed in color online but in black and white in the print edition.

Abbreviation used in this paper: LDA = linear discrimination analysis.

measurements are a poor substitute for intracranial brain and fluid volumes and are most effective during the first 10–24 months of life.<sup>1,32</sup> Ventricular horn indices, ventricle/brain ratios, and cortical thickness measurements are often used clinically as substitutes for head circumference.<sup>24,27</sup> All of these measures, however, fail to fully characterize morphological changes in hydrocephalic development and do not capture total brain volume.

This study attempts to understand brain and fluid volume dynamics in normal development and to contrast these with an experimental model of hydrocephalus. We define hydrocephalus as the accumulation of CSF at greater than 3 SDs above normative averages in the developing brain. To meet this definition, we need normative growth curves, which we will define in this paper. By defining normal volume dynamics, we can explore the feasibility of an improved framework for a more rational design of therapy than is currently provided by the use of head circumference or linear measurements from brain imaging. Our hypothesis is that achieving normal brain volume growth is likely more important than fluid volume per se in the achievement of normal cognitive function in children. The ultimate goal in the treatment of pediatric hydrocephalus is to create an intracranial environment for the brain to properly develop. Therefore, assessing both dynamic brain and fluid volumes will be important in improving the diagnosis and management of pediatric hydrocephalus.

## Methods

All animal procedures were approved by Penn State University's institutional animal care and use committees.

### *Induction of Hydrocephalus*

Fourteen-day-old C57BL/6 mice (Harlan Labs) were anesthetized (2% isoflurane in 0.5 L/minute O<sub>2</sub>). Ten microliters of sterilized kaolin solution, composed of 250 mg kaolin and 50  $\mu$ l Magnevist contrast agent (Bayer Healthcare) per milliliter of 0.9% saline, were injected percutaneously using aseptic technique into the cisterna magna with a 100- $\mu$ l Hamilton syringe and 30-gauge needle. Animals were observed daily postinjection and body weights were obtained prior to imaging. A total of 35 mice from 6 litters were injected.

### *Magnetic Resonance Imaging*

All imaging was performed on an 89-mm vertical wide-bore 14.1-T unit (Varian, Inc.) with Direct Drive technology. The gradient system had an inner diameter of 55 mm and maximum field strength of 550 mT/m. A T2-weighted spin echo pulse sequence (TR 5000 msec, TE 30 msec) with a custom-built surface resonator (2  $\times$  1.7 mm) was used to achieve high contrast between the brain tissue and fluid. Partial Fourier imaging was used, with 75% k-space coverage (96 points) in the phase-encode direction; 160 complex data points were acquired in the readout direction, and the data were zero-filled to 320  $\times$  256. Slice thickness was 200  $\mu$ m, while in-plane resolution was between 81 and 94  $\mu$ m, depending on the FOV used. The slice acquisition was interleaved with no

gap between the slices. Four averages were acquired for a total scan time of 32 minutes. Control mice were littermates that were not injected. The control mice were imaged once per week from 2 to 4 weeks of age, then every other week from 4 to 12 weeks of age. Hydrocephalic mice underwent imaging just before the kaolin injection at 2 weeks of age, 2 days postinjection, and then every 3–5 days whenever possible.

### *Image Processing and Volumetric Analysis*

The images were imported into AMIRA 4.1 (Visage Imaging) for processing and segmentation. A 2D 3-by-3 median filter was applied to the images before segmentation. The AMIRA system uses semiautomatic segmentation tools such as region growing, edge tracing, and connected thresholding tools, as well as a manual pixel selection tool, all of which were used to segment data in this study. The total brain volume was generated by segmenting the surface area for each slice, beginning rostrally with the olfactory bulb region and ending caudally in the brainstem on the slice showing the most ventral portion of the cerebellum. Fluid from the lateral, third, and fourth ventricles was included in this segmentation. An atlas<sup>14</sup> was used to determine correct tissue and fluid classification, and the results were checked by a neurosurgery expert and an MR imaging expert.

In addition to calculating brain and fluid volumes of the hydrocephalic and normal mice, we calculated the frontal and occipital horn ratio<sup>24</sup> and head circumference from the images. The frontal and occipital horn ratio was calculated as the sum of the maximal width of the frontal horn and occipital horn of the lateral ventricles divided by twice the maximum brain width taken in an axial slice at the level of the cerebral aqueduct. On the same axial slice, head circumference was estimated as the circumference of the brain and fluid in the cranial cavity. These measures were calculated for the final data set acquired for each normal and hydrocephalic mouse. Head circumference was also calculated for normal 3-week-old mice to compare with the hydrocephalic mice of the same age. However, it was not possible to measure the frontal and occipital horn ratio in the mice at this age because the fluid could not be observed in the occipital horn in a brain this immature.

### *Data Analysis*

In 1936 Roland Fisher<sup>12</sup> created a method of multivariable discrimination to help classify data that had more than 1 measurement and that came from more than 1 group of items. Fisher's problem was motivated by iris flowers. He had petal and sepal length and width measurements of each of 3 species (50 samples each). He was able to find the optimal way of adding these 4 measurement variables together so that he could clearly show that these sets of measurements could separate and classify each species type. Indeed, the method provides a recipe to measure a new item, weight the measurements, and optimally classify the likely species for this out of sample data. A similar biological example, with only a few items, was shown by Bernhard Flury using midges measured for antenna and

## Dynamics of brain and CSF growth in hydrocephalic mice

wing length.<sup>13,15</sup> We have refined this method, to take into account modern numerical computer algorithms<sup>28</sup> (Fisher did all of his work on a hand calculator), and we employ this numerically stable form of LDA in what follows.

We used LDA to test the classification of hydrocephalic data into 2 separate groups: 1) hydrocephalic mice with abnormal brain enlargement and 2) hydrocephalic mice with brain growth consistent with normal controls. In this study the variables used for analysis are brain volume and ventricle volume. For each hydrocephalic mouse, the final brain and ventricle volume measurements were normalized by the age-matched control brain and ventricle volumes. This resulted in a  $9 \times 2$  matrix,  $Y$ , consisting of a single brain and single ventricle volume measurement for each of 9 hydrocephalic mice. The data from each mouse were classified into either Group 1 for hydrocephalic mice with abnormal brain enlargement or Group 2 for hydrocephalic mice with normal brain growth.

Wilks test statistic,  $W$ , was used to test for the significance of the classification. This likelihood ratio tests the hypothesis,  $H_0$ , that each group mean,  $\mu_k$ , is equal:

$$H_0 : \mu_1 = \mu_2 = \dots = \mu_k [1]$$

In addition to testing the significance of the rejection of  $H_0$ , the Wilks statistic is also used to test random combinations of regrouping the data with a bootstrapping method.<sup>11,13,28</sup> This is employed to prove that the grouping defined prior to the LDA is unlikely to have occurred by chance. The Wilks statistic for each permutation of the data is compared with the Wilks statistic for the originally defined classification. The bootstrap probability,  $P_b$ , is the probability that the original classification would occur randomly and is given by

$$P_b = \frac{N_{less} + 1}{N_{perm} + 1} [2]$$

where  $N_{less}$  is the number of groupings found with a Wilks statistic less than or equal to the original  $W$  statistic calculated, and  $N_{perm}$  is the number of permutations. This calculation includes the original grouping as one of the permutations in addition to those calculated in the randomization of the bootstrap algorithm; thus adding one more permutation with a Wilks statistic equal to the original grouping. This is accomplished by adding 1 to both the numerator and denominator of Equation 2.

The LDA was also used to test the ability of normalized brain volume, normalized ventricle volume, frontal and occipital horn ratio, and head circumference to discriminate between the patterns of observed hydrocephalic development.

### Results

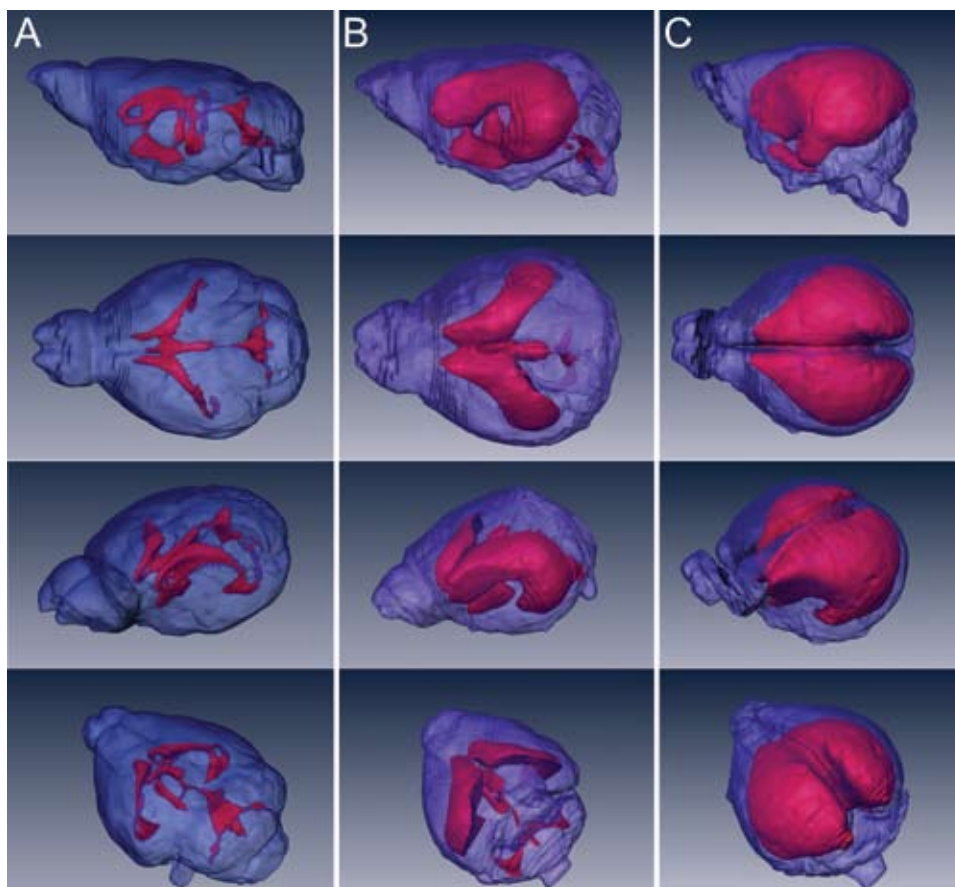
Ventricular enlargement was seen in the first postinjection MR images obtained in hydrocephalic mice—that is, within 2 to 3 days of injection. If the injection did not result in a clearly hydrocephalic mouse by the first imaging session, subsequent imaging revealed that the mouse never became hydrocephalic. The hydrocephalic mouse's head often became visibly dome shaped, and the mice generally weighed less and were more lethargic



Fig. 1. Photograph of 4-week-old normal (left) and hydrocephalic (right) mice from the same litter. Note the smaller size and dome-shaped head of the hydrocephalic mouse.

than their littermates (Fig. 1). Volumetric reconstructions of 3 mice—a 12-week-old normal mouse, a 4-week-old moderately hydrocephalic mouse, and a 4-week-old severely hydrocephalic mouse—are shown in Fig. 2. Meeting the criteria of hydrocephalus, the substantial increase in fluid can be seen in these reconstructions. Of the 35 mice injected, 9 successfully acquired hydrocephalus, 17 survived the injection procedure but did not acquire hydrocephalus, and 9 did not survive the injection.

Each hydrocephalic mouse exhibited differences in the growth of brain and fluid. The 3 major categories of development are shown in Fig. 3: normal controls (Rows A and B), hydrocephalus without edema (Row C), and hydrocephalus with edematous brain (Rows D and E). Examples of mild, moderate, and severe hydrocephalus are also shown in these examples (Rows D, C, and E, respectively). Rows A and B show normal mice at ages 4 and 12 weeks. Row C shows a mouse with hydrocephalus of moderate severity at 24 days of age; the lateral, third, and fourth ventricles are all enlarged. Row D shows the hydrocephalic mouse with the smallest ventricular volume; at 26 days all ventricles were larger than normal, and substantial edema was present in the forceps minor and forceps major of the corpus callosum, the external capsule, and around the dorsal hippocampal commissure. Edema was seen in the images as increased signal intensity due to longer T2 signal values. As seen in Row D of Fig. 3, hydrocephalus often generates a cavum septum pellucidum, or fifth ventricle.<sup>6,8,16</sup> Row E shows the most severely hydrocephalic mouse; at 28 days of age the remarkable ventricular size was accompanied by periventricular edema as well as fused lateral ventricles. Interestingly, the fourth ventricle is not seen, suggesting the obstruction in this mouse was at the aqueduct of Sylvius above the cisterna magna. In this particular case, the ventricular system later ruptured, leading to a normalization of brain and ventricle volume, as well as the loss of periventricular edema (Fig. 4). The images not only show decreased brain volume from the disappearance of edema but a 40% increase in cortical thickness (measured from the middle slice of the upper and lower rows shown in Fig. 4). Unfortunately, this mouse did not survive suffi-



**FIG. 2.** Volumetric reconstruction of the segmented MR images obtained in a 12-week-old normal mouse (**Column A**), a moderately hydrocephalic mouse at 4 weeks (**Column B**), and a severely hydrocephalic mouse at 4 weeks (**Column C**). *Blue* designates brain and *red* indicates ventricular fluid. A lateral view (**Row 1**), dorsal view (**Row 2**), and angled views, as seen from the anterior (**Row 3**) and posterior (**Row 4**), of the same mice through each column is shown. Note the dramatic increases in fluid and the more rounded shapes of the hydrocephalic brains.

ciently long after this catastrophic ventricular rupture to permit further serial imaging.

Two very different patterns of response were seen in hydrocephalic mice compared with normative growth curve data (Fig. 5). In one pattern (3 mice), brain volume growth was normal despite the accumulation of CSF and head enlargement. In this pattern, the mice showed no signs of periventricular edema. In the second pattern (6 mice), brain volume enlarged abnormally as parenchymal edema increased. As defined by hydrocephalus, ventricle volume was greater than normal in both patterns. In this second pattern of pathological brain enlargement, the 1 case of a spontaneous rupture of the ventricular system led to a normalization of brain volume, ventricle volume, and cortical thickness.

A ratio of the final brain and intraventricular CSF volumes for each hydrocephalic mouse to the estimated age-matched normal volumes was calculated for the LDA (Table 1). The normal volume estimations were calculated from a natural log least-squares fit to the normal growth curve data. The coefficient of multiple determination,  $R^2$ , is the ratio of the regression sum of squares to the total sum of squares.<sup>26</sup> The  $R^2$  values calculated for the normal brain and ventricle volume fitted curves are 0.82

and 0.89, respectively. The groups were determined based on the presence (Group 1) or absence (Group 2) of brain edema. This classification corresponded with abnormal brain enlargement (Group 1) or brain growth consistent with normal (Group 2).

The matrix  $Y$  is the hydrocephalic brain (first column) and ventricle (second column) volumes normalized to the age-matched normal data. The data are classified into  $Y_1$  and  $Y_2$  corresponding to Groups 1 and 2, respectively:

$$Y_1 = \begin{pmatrix} 1.09 & 33.29 \\ 1.09 & 32.24 \\ 1.26 & 22.48 \\ 1.23 & 104.1 \\ 1.18 & 5.47 \\ 1.14 & 15.64 \end{pmatrix}$$

$$Y_2 = \begin{pmatrix} 1.03 & 41.71 \\ 0.97 & 28.77 \\ 0.99 & 17.89 \end{pmatrix}$$

## Dynamics of brain and CSF growth in hydrocephalic mice

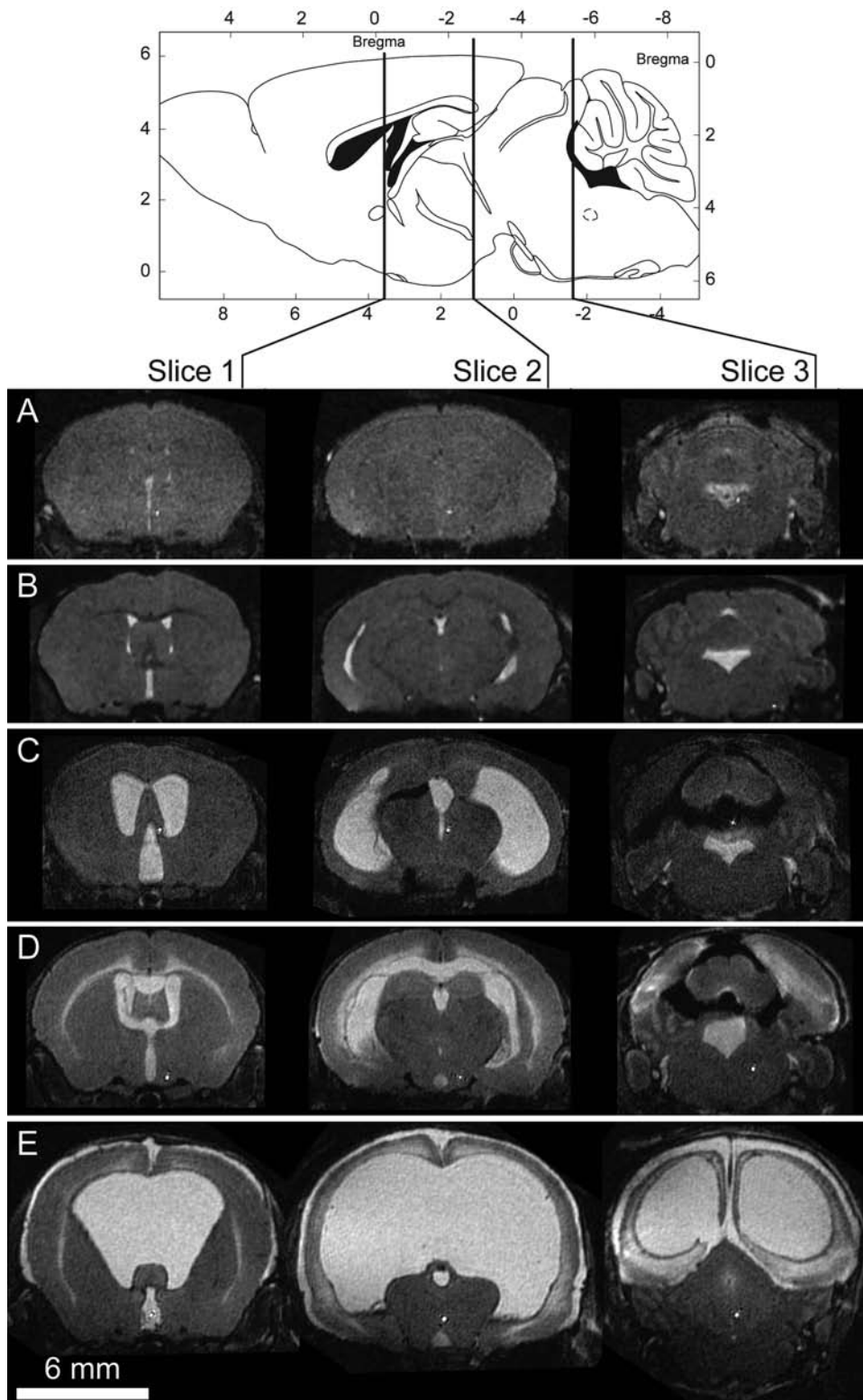


**FIG. 3.** Coronal T2-weighted MR images and related drawing. The locations of the 3 slices are indicated in the diagram at the top. **Rows A and B:** The same normal mouse is shown at 4 weeks and 12 weeks of age, respectively. The lateral and third ventricles are just seen at 4 weeks and are well defined by 12 weeks of age. **Row C:** A moderately hydrocephalic mouse with normal brain volume (lacking signs of periventricular edema) at 24 days of age. **Rows D and E:** The mildest and most severely hydrocephalic mice at 26 days and 28 days of age, both with substantial periventricular edema. Although edema might be due to a transcortical pressure gradient, it is not dependent on the size of the ventricles alone. The drawing of the mouse brain is reprinted with permission from Elsevier (Franklin KBJ, Paxinos G: **The Mouse Brain in Stereotaxic Coordinates, 3rd Ed.**, 2007).

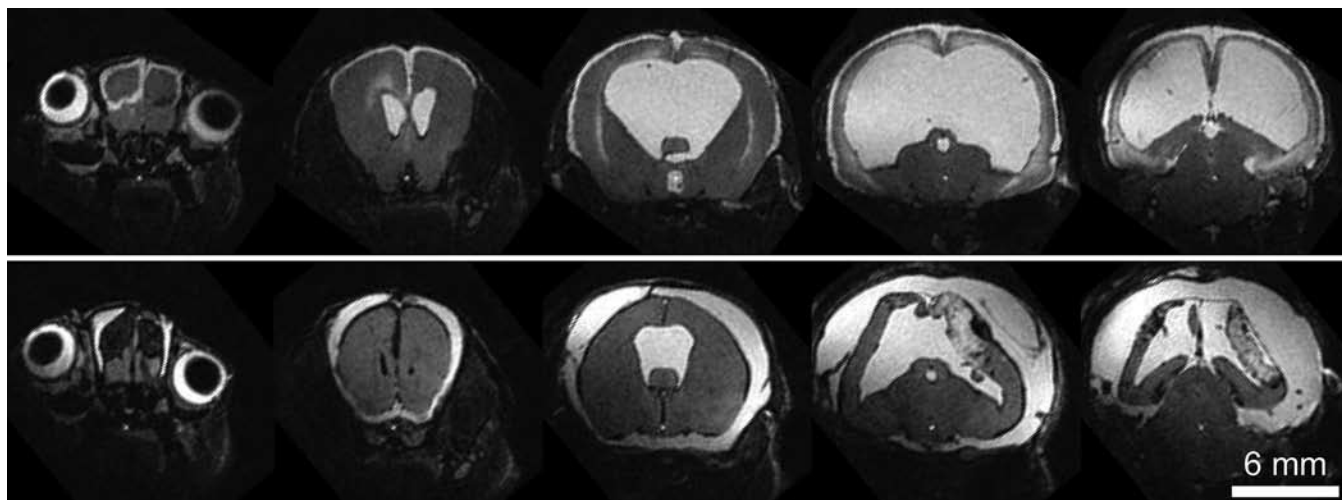


**Fig. 4.** Coronal T2-weighted MR images of the same severely hydrocephalic mouse at 4 weeks of age (**upper**) and 5 weeks of age (**lower**). Each slice is 200- $\mu$ m thick, and every third slice is shown. The lateral ventricles ruptured between the imaging sessions on week 4 and 5. After the rupture, the intraventricular fluid volume substantially decreased and extraventricular fluid volume increased. Cortical thickness increased 40% (measured from the third slice) despite a drop in total brain volume. Signs of periventricular edema are no longer present, suggesting that a transcortical pressure gradient was responsible for the presence of edema.

The means  $\bar{y}_j$  and covariance matrices  $\hat{\psi}_j$ , for groups  $j = 1, 2$  are calculated as follows:

$$\bar{y}_1 = \begin{pmatrix} 1.16 \\ 35.54 \end{pmatrix}; \hat{\psi}_1 = \begin{pmatrix} 0.0043 & 0.6771 \\ 0.6771 & 1031.9 \end{pmatrix}$$

$$\bar{y}_2 = \begin{pmatrix} 1.00 \\ 29.46 \end{pmatrix}; \hat{\psi}_2 = \begin{pmatrix} 0.0006 & 0.1678 \\ 0.1678 & 94.8507 \end{pmatrix}$$

Note that  $\hat{\psi}_j$  are not unbiased<sup>13</sup> and are calculated with,  $N_1 = 6$  and  $N_2 = 3$ . The total variability  $\psi$  is the sum

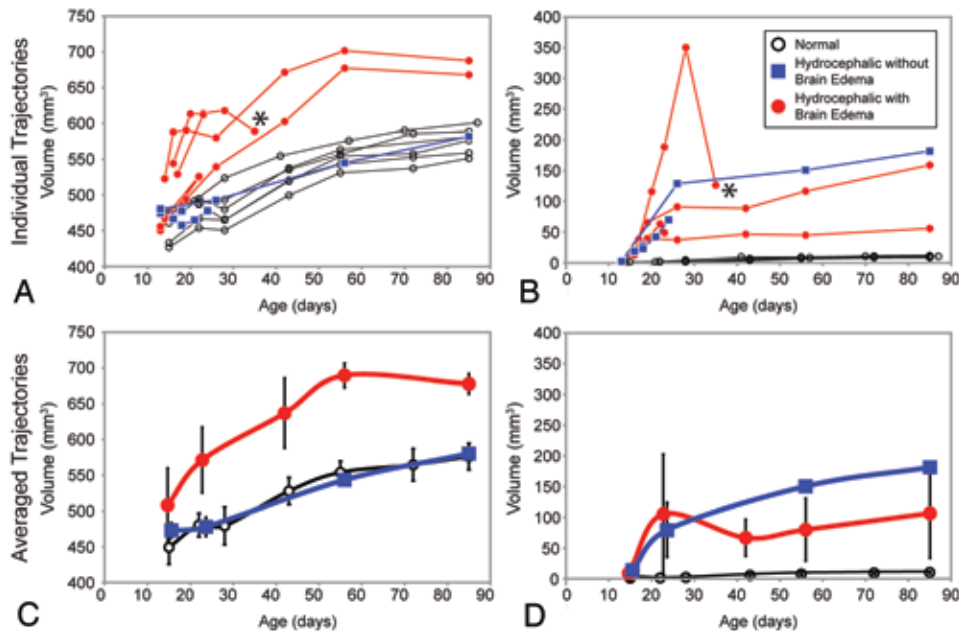


**Fig. 5.** Line graphs demonstrating the development of brain and ventricle volumes in all mice showing the development for each mouse individually (**A and B**) and the data averaged for each group (normal [6 mice], hydrocephalic without brain edema [3 mice], and hydrocephalic with brain edema [6 mice]) (**C and D**). In **C** and **D**, the volume measurements of the solitary survivor of hydrocephalus without brain edema are shown without averaging. Ventricle volumes of all hydrocephalic mice are significantly larger than those with normal brains, but brain volumes are only different from normal in those hydrocephalic mice with edematous brain. In no case was the total brain volume of a hydrocephalic mouse smaller than normal. The data points with asterisks occurred after the ventricular rupture shown in Fig. 4. After the rupture, the brain and ventricle volumes decrease toward the normal curves. The data points marked with asterisks were excluded from the averaged graphs. The error bars in the averaged graphs display 1 SD above and below the mean. In **D**, the normal ventricle volume curve is plotted at 1 SD above the mean (the error bars are still centered around the mean) to adequately show the large differences in volume compared with the hydrocephalic mice.

# Dynamics of brain and CSF growth in hydrocephalic mice

of the within-group,  $\hat{\psi}_w$  and the between-group,  $\hat{\psi}_B$ , variabilities.

$$\hat{\psi}_w = \begin{pmatrix} 0.0031 & 0.5073 \\ 0.5073 & 719.5357 \end{pmatrix}$$

$$\hat{\psi}_B = \begin{pmatrix} 0.0060 & 0.2222 \\ 0.2222 & 8.2242 \end{pmatrix}$$

The prior probabilities of a measurement belonging to Group 1 or 2 are  $\hat{\pi}_1 = 2/3$  and  $\hat{\pi}_2 = 1/3$ . Since the rank of  $\hat{\psi}_B$  is  $m = \min(p, k - 1) = 1$ , where  $p$  is the number of variables (2), and  $k$  is the number of groups (2), there is at most 1 canonical discriminant function. The 2 eigenvalues of  $\hat{\psi}_B$  are  $\lambda_1 = 2.104$  and  $\lambda_2 \approx 0$ . The value of  $\lambda_1$  can be interpreted as the ratio of normalized between-group variance to within-group variance, meaning the normalized between-group variance is approximately 2 times the within-group variance. The value of  $\lambda_2$  confirms that the data can be best classified by a linear combination of only the first discriminant function. The canonical variate,  $z$ , where  $z = Y * \hat{\gamma}$ , is defined by the coefficients of the first discriminant function,  $\hat{\gamma}$ :

$$\hat{\gamma} = \begin{pmatrix} -19.1194 \\ 0.0107 \end{pmatrix}$$

$$z = -19.1194 * y_1 + 0.0107 * y_2$$

where  $y_1$  is the normalized brain volume measurement and  $y_2$  is the normalized ventricle volume measurement for an individual mouse.

The hydrocephalic mice were clearly separated by the normalized brain volume and, to a lesser extent, by the normalized ventricle volume (Fig. 6). All of the data points have posterior probabilities close to 100%, except for the 2 hydrocephalic mice with abnormal brain enlargement plotted close to the discrimination line, which have posterior probabilities of 71 and 76%. The Wilks statistic calculated for the entire data set was 0.32, less than the value of 0.36 expected by the chi-square distribution for  $W$  (DF = 2,  $p = 0.01$ ). Normalized brain volume alone successfully discriminates between the 2 patterns of hydrocephalus ( $W = 0.34$ ,  $p < 0.01$ , chi-square distribution), whereas normalized ventricle volume alone cannot discriminate these 2 patterns of hydrocephalus ( $W = 0.99$ ).

The classification of data into hydrocephalus with excessive brain enlargement or normal brain volume growth was checked by randomly mixing the group assignments with a bootstrap method. Figure 7 shows the results for 1000 random permutations of the data. The results are shown as a histogram of the frequency of the Wilks statistic for each permutation, and the  $W$  values of the original data are marked with an asterisk. There were only 29 other ways found to regroup the data to obtain a better  $W$  statistic, leading to a 3.0% probability that the prior classification was obtained by chance.

Measurements of frontal and occipital horn ratio and head circumference are shown in Fig. 8. The frontal and occipital horn ratio was able to separate normal and hydrocephalic mice ( $W = 0.23$ ,  $p < 0.01$  by chi-square distribution) but was not able to discriminate between the 2 patterns of hydrocephalus, irrespective of whether they were analyzed together ( $W = 0.90$ ) or separated by age ( $W = 0.96$  at 3 weeks and  $W = 0.68$  at 12 weeks). Head circumference was able to separate normal and hydrocephalic mice at 12 weeks of age ( $W = 0.16$ ,  $p < 0.01$  by chi-square distribution), but was unable to separate the mice at 3 weeks of age ( $W = 0.84$ ). Head circumference also failed to separate the 2 patterns of hydrocephalus when analyzed separately by age ( $W = 0.66$  at 3 weeks and  $W = 0.58$  at 12 weeks) or when analyzed all together ( $W = 0.81$ ).

## Discussion

This study is, to our knowledge, the first serial quantification of the growth of brain and cerebral ventricle volumes in normal and hydrocephalic development. Hydrocephalus was induced by a percutaneous injection of kaolin into the cisterna magna, and mice were imaged with high-field MR imaging. Despite the common use of ventricular size, cortical thickness, and ratios of ventricle to linear brain measurements, brain volume has not been used in an attempt to understand the development of hydrocephalus in animals or humans.

Two very different patterns of response were seen in the hydrocephalic mice, each correlating with the absence or presence of edematous brain. In the first pattern, the hydrocephalic mice displayed brain growth consistent with normal control mice and did not have any obvious signs of edematous brain. In the second pattern, the hydrocephalic

TABLE 1: Summary of data used for the Fisher LDA

Group	Hydrocephalic (mm <sup>3</sup> )		Age (days)	Normal (mm <sup>3</sup> )		Hydrocephalic/Normal	
	Brain	CSF		Brain	CSF	Brain	CSF
1	526.5	62.86	22	483.0	1.89	1.09	33.29
1	524.3	60.88	22	483.0	1.89	1.09	32.24
1	612.2	48.56	23	486.3	2.16	1.26	22.48
1	618.2	350.3	28	501.2	3.36	1.23	104.10
1	687.7	55.54	85	585.1	10.16	1.18	5.47
1	667.8	158.9	85	585.1	10.16	1.14	15.64
2	482.6	27.55	18	467.8	0.66	1.03	41.71
2	477.8	69.65	24	489.5	2.42	0.97	28.77
2	580.1	181.7	85	585.1	10.16	0.99	17.89

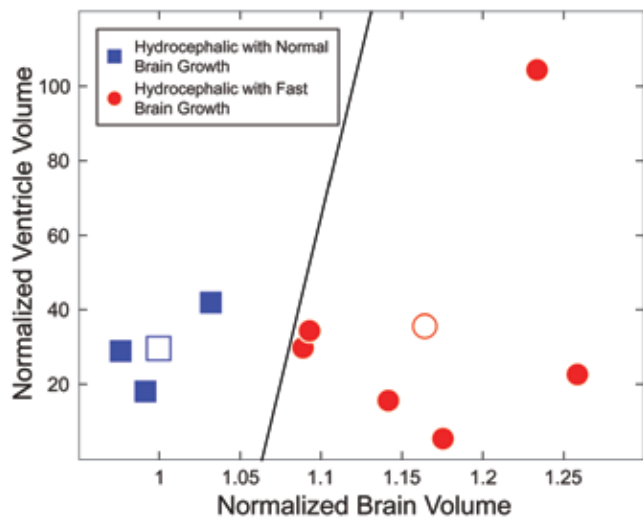


Fig. 6. Graph showing hydrocephalic mice classified by the linear discrimination function. The brain and ventricle volumes are normalized by the age-matched normal volumes. The black line dividing the plot is the calculated cutoff point for classification. The open circle and square show the mean values of each group. Although the data are best classified by a combination of the brain and ventricle volumes, the brain volume alone is able to discriminate between the 2 groups, whereas ventricle volume alone is not.

mice showed brain volumes increasing faster than normal and presented with substantial edematous brain, seen as increased T2 signal in the MR images. There is a well-characterized linear relationship between T2 signal value and water content.<sup>2,3</sup> Additionally, in recent studies of kaolin-induced hydrocephalus with infant rats and mice, increased T2 signal was confirmed as edema by histological methods.<sup>5,19</sup> In our study, the increased T2 signal is therefore most consistent with extracellular edema. The edematous tissue was seen most notably in the periventricular white matter, as reported elsewhere.<sup>5,9,17,19,23</sup> White matter is made up of bundles of axons and oligodendrocytes and lacks the astrocytic processes that hold together gray matter structures. This may allow fluid to enter and expand the extracellular spaces of these structures.<sup>23</sup> In this second pattern, the most severe case of hydrocephalus resulted in a spontaneous ventricular rupture, allowing much of the fluid to escape the ventricular system, acting therapeutically much like an endoscopic ventriculostomy. After the rupture, the

brain volume and ventricular volume decreased toward the normal curve, and the edema was no longer seen. Additionally, cortical mantle thickness increased while brain volume decreased. Cortical thickness can therefore change inversely to that of the brain volume it is supposed to estimate. This case demonstrates experimental evidence of a correlation between abnormal brain size and edema in the hydrocephalic brain and suggests that a transmante pressure gradient was responsible for the presence of edema. However, the presence of edema is not dependent on ventricle size alone, as both the mildest and most severely hydrocephalic mice both showed signs of edematous brain.

In no case did the hydrocephalic brain volume grow at a rate slower than normal, suggesting that in these young mice, as in humans,<sup>32</sup> the skull was able to expand to compensate for the increased ventricle and brain sizes. Furthermore, these data demonstrate a clear time window in early hydrocephalus when the brain can be expanded without atrophy and volume loss.

The differences in the 2 responses of hydrocephalic brain volume growth were confirmed using LDA and a bootstrap method.<sup>12,13,26,28</sup> The weighting of the discriminant function shows that the groups are best classified by a combination of both normalized brain and ventricle volume. Nevertheless, ventricle volume alone is not an effective discriminator between these 2 hydrocephalic dynamics, demonstrating the added value of brain volume measurements by MR imaging or CT.

Current clinical measurements of head circumference and frontal and occipital horn ratio were also used to analyze the data. Head circumference, as estimated in this study by brain circumference, was able to discriminate between normal and hydrocephalic mice, but only in the 12-week-old mice. Discrimination was not possible at 3 weeks even though the ventricle volumes were already 20–90 times the volume of normal ventricles. Based on the results presented here, the rate at which changes in head circumference show signs of hydrocephalus is on a time scale much slower than one would desire in clinical practice. The frontal and occipital horn ratio was able to discriminate between normal and hydrocephalic mice at both 3 and 12 weeks of age because frontal and occipital horn ratio is an effective estimator of ventricle volume.<sup>24</sup> However, neither measure was able to discriminate between the 2 patterns of hydrocephalus. In this animal model, brain vol-

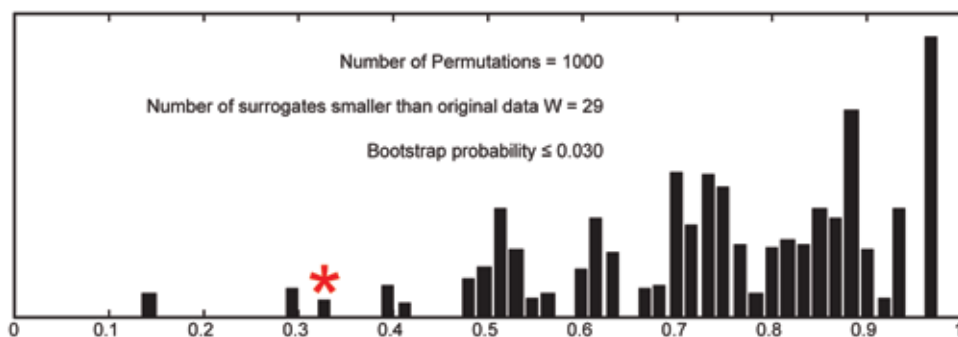


Fig. 7. The bootstrap results for 1000 permutations of reclassification of the data plotted as a histogram of the Wilks statistic. The Wilks statistics for the original data are marked with an asterisk. Only 2 unique permutations (total 29) of the data gave better Wilks statistics, yielding a 3% probability that the data classified were obtained by chance.

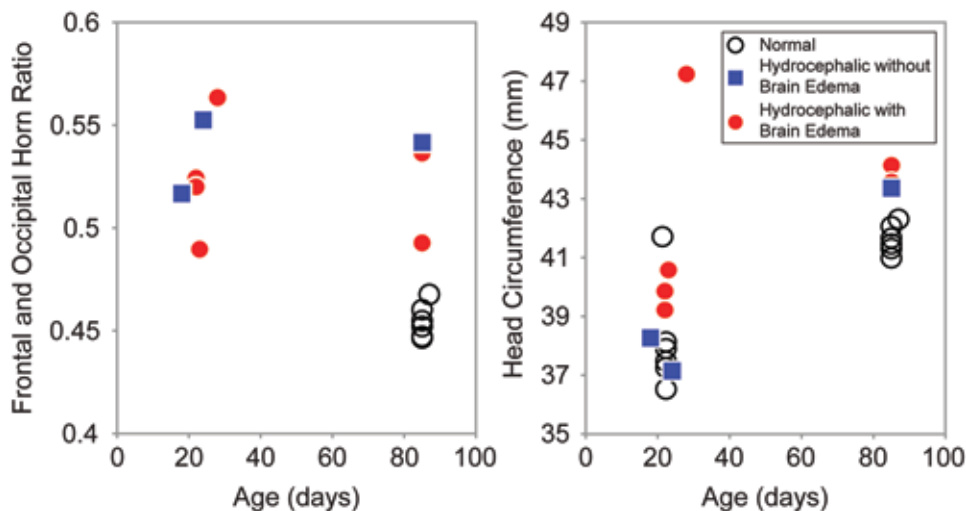


Fig. 8. Frontal and occipital horn ratio and head circumference plotted as a function of age for normal and hydrocephalic mice. The frontal and occipital horn ratio is able to discriminate between normal and hydrocephalic mice at 12 weeks. It was not possible to measure the frontal and occipital horn ratio for normal mice at 3 weeks, but the 12-week normal frontal and occipital horn ratio is still significantly different than that in the hydrocephalic mice at 3 weeks. Head circumference is able to discriminate between normal and hydrocephalic mice at 12 weeks but not at 3 weeks. Neither the frontal and occipital horn ratio nor head circumference is able to discriminate between the 2 patterns of hydrocephalus.

ume was the only effective discriminator of the 2 patterns of hydrocephalus. Additionally, the frontal and occipital horn index, which correlates inversely with cortical mantle thickness, consistently increases in the hydrocephalic mice whether the brain is increasing in size or not. Normal brain growth is the target of clinical treatment, but in those hydrocephalic mice that showed normal brain growth there was still a decreased mantle thickness. We speculate that it is likely, however, that the hydrocephalic brain with increased volume due to edema will lead to worse cognitive development and clinical outcomes.

This present study suggests that neonatal hydrocephalus can have very different patterns of volume growth. Current evaluation methods show decreases in cortical thickness and increases in ventricle to brain ratios<sup>4,5,7,17,19,22,29</sup> but do not reveal brain volumes directly. Our finding that the brain increases in size faster than normal is impossible to observe with measures currently in clinical use.

Total brain volume is of substantial importance in understanding hydrocephalus, as the overall goal of treating pediatric hydrocephalus is to enable normal brain development, which is not equivalent to decreasing fluid volumes. The patient's brain growth, water content, and turgor should be as great a concern as the volume of CSF within the cranial cavity. Although ventricular volume has been considered to be the gold standard for following hydrocephalus,<sup>24</sup> it does not offer a direct indication of cognitive function. We have learned to be more cautious in treating patients with achondroplastic dwarfism because most have relatively preserved cognitive function in the setting of mildly to moderately dilated ventricles.<sup>20</sup> Because many children with enlarged ventricles appear to develop normally, both with and without achondroplasia, the standard for diagnosis and treatment becomes the response to treatment itself.<sup>21,31</sup> Although hydrocephalus has historically been seen as a simple imbalance of CSF production and absorption, more recently it is being rec-

ognized as a more complex brain disorder composed of neuronal and glial injury.<sup>31</sup>

### Conclusions

Our findings demonstrate the feasibility of constructing normative curves of brain and fluid growth as complements, or alternatives, to head circumference normative curves. By observing brain volumes in this animal model, we were able to measure distinct patterns of normal brain growth and abnormal brain enlargement compared with normative growth, measures that are more likely linked to cognitive development than fluid volumes alone. Indeed, both excessive brain volume due to edema and eventual decrease in brain volume due to the prolonged effects of elevated pressure are states to avoid through suitable clinical management. In order for brain volume assessment to be implemented clinically in the diagnosis and management of hydrocephalus, the measurement must be automated with a reliable and accurate method. A dynamic model of brain and CSF growth in normal and hydrocephalic humans would offer the possibility for a more rational design of therapy aimed at optimizing brain growth and associated cognitive capacity.

### Disclosure

The authors report no conflict of interest concerning the materials or methods used in this study or the findings specified in this paper.

Author contributions to the study and manuscript preparation include the following. Conception and design: all authors. Acquisition of data: Mandell, Neuberger. Analysis and interpretation of data: all authors. Drafting the article: Schiff, Mandell. Critically revising the article: all authors. Reviewed final version of the manuscript and approved it for submission: all authors. Statistical analysis: Schiff, Mandell, Drapaca, Webb. Administrative/technical/material support: Schiff, Neuberger, Drapaca, Webb. Study supervision: Schiff, Neuberger, Drapaca, Webb.

## References

1. American Academy of Pediatrics Committee on Practice and Ambulatory Medicine, Bright Futures Steering Committee: Recommendations for preventive pediatric health care. **Pediatrics** **105**:645–646, 2000
2. Barnes D, McDonald WI, Johnson G, Tofts PS, Landon DN: Quantitative nuclear magnetic resonance imaging: characterization of experimental cerebral oedema. **J Neurol Neurosurg Psychiatry** **50**:125–133, 1987
3. Bederson JB, Bartkowski HM, Moon K, Halks-Miller M, Nishimura MC, Brant-Zawadski M, et al: Nuclear magnetic resonance imaging and spectroscopy in experimental brain edema in a rat model. **J Neurosurg** **64**:795–802, 1986
4. Boillat CA, Jones HC, Kaiser GL, Harris NG: Ultrastructural changes in the deep cortical pyramidal cells of infant rats with inherited hydrocephalus and the effect of shunt treatment. **Exp Neurol** **147**:377–388, 1997
5. da Silva Lopes L, Slobodian I, Del Bigio MR: Characterization of juvenile and young adult mice following induction of hydrocephalus with kaolin. **Exp Neurol** **219**:187–196, 2009
6. Dandy WE: Congenital cerebral cysts of the cavum septi pellucidi (fifth ventricle) and cavum vergae (sixth ventricle). **Arch Neurol Psychiatry** **25**:44–66, 1931
7. Dandy WE: Experimental hydrocephalus. **Ann Surg** **70**:129–142, 1919
8. Del Bigio MR: Future directions for therapy of childhood hydrocephalus: a view from the laboratory. **Pediatr Neurosurg** **34**:172–181, 2001
9. Del Bigio MR, Crook CR, Buist R: Magnetic resonance imaging and behavioral analysis of immature rats with kaolin-induced hydrocephalus: pre- and postshunting observations. **Exp Neurol** **148**:256–264, 1997
10. Drake JM: The surgical management of pediatric hydrocephalus. **Neurosurgery** **62 Suppl 2**:633–642, 2008
11. Efron B, Tibshirani RJ: **An Introduction to the Bootstrap. Monographs on Statistics and Applied Probability, Vol 57.** New York: Chapman & Hall/CRC, 1993
12. Fisher RA: The use of multiple measurements in taxonomic problems. **Ann Eugen** **7**:179–188, 1936
13. Flury B: **A First Course in Multivariate Statistics.** New York: Springer, 1997
14. Franklin KBJ, Paxinos G: **The Mouse Brain in Stereotaxic Coordinates, ed 3.** New York: Academic Press, 2007
15. Grogan WL Jr, Wirth WW: A new American genus of pre-deaceous midges related to Palpomyia and Bezzia (Diptera: Ceratopogonidae). **Proc Biol Soc Wash** **94**:1279–1305, 1981
16. Hankin MH, Schneider BF, Silver J: Death of the subcallosal glial sling is correlated with formation of the cavum septi pellucidi. **J Comp Neurol** **272**:191–202, 1988
17. Harris NG, Jones HC, Williams SCR: MR imaging for measurements of ventricles and cerebral cortex in postnatal rats (H-Tx strain) with progressive inherited hydrocephalus. **Exp Neurol** **118**:1–6, 1992
18. Kestle JR: Pediatric hydrocephalus: current management. **Neurol Clin** **21**:883–895, vii, 2003
19. Khan OH, Enno TL, Del Bigio MR: Brain damage in neonatal rats following kaolin induction of hydrocephalus. **Exp Neurol** **200**:311–320, 2006
20. King JAJ, Vachhrajani S, Drake JM, Rutka JT: Neurosurgical implications of achondroplasia. A review. **J Neurosurg Pediatr** **4**:297–306, 2009
21. Lewin R: Is your brain really necessary? **Science** **210**:1232–1234, 1980
22. Li J, McAllister JP II, Shen Y, Wagshul ME, Miller JM, Egnor MR, et al: Communicating hydrocephalus in adult rats with kaolin obstruction of the basal cisterns or the cortical subarachnoid space. **Exp Neurol** **211**:351–361, 2008
23. McLone DG, Bondareff W, Raimondi AJ: Brain edema in the hydrocephalic hy-3 mouse: submicroscopic morphology. **J Neuropathol Exp Neurol** **30**:627–637, 1971
24. O'Hayon BB, Drake JM, Ossip MG, Tuli S, Clarke M: Frontal and occipital horn ratio: a linear estimate of ventricular size for multiple imaging modalities in pediatric hydrocephalus. **Pediatr Neurosurg** **29**:245–249, 1998
25. Raimondi AJ, Bailey OT, McLone DG, Lawson RF, Echeverry A: The pathophysiology and morphology of murine hydrocephalus in Hy-3 and Ch mutants. **Surg Neurol** **1**:50–55, 1973
26. Rencher AC: **Methods of Multivariate Analysis, ed 2.** New York: John Wiley & Sons, 2002
27. Rizvi R, Anjum Q: Hydrocephalus in children. **J Pak Med Assoc** **55**:502–507, 2005
28. Schiff SJ, Sauer T, Kumar R, Weinstein SL: Neuronal spatiotemporal pattern discrimination: the dynamical evolution of seizures. **Neuroimage** **28**:1043–1055, 2005
29. Slobodian I, Krassioukov-Enns D, Del Bigio MR: Protein and synthetic polymer injection for induction of obstructive hydrocephalus in rats. **Cerebrospinal Fluid Res** **4**:9, 2007
30. Tada T, Kanaji M, Kobayashi S: Induction of communicating hydrocephalus in mice by intrathecal injection of human recombinant transforming growth factor-beta 1. **J Neuroimmunol** **50**:153–158, 1994
31. Williams MA, McAllister JP, Walker ML, Kranz DA, Bergsneider M, Del Bigio MR, et al: Priorities for hydrocephalus research: report from a National Institutes of Health-sponsored workshop. **J Neurosurg** **107 (5 Suppl)**:345–357, 2007
32. Zahl SM, Wester K: Routine measurement of head circumference as a tool for detecting intracranial expansion in infants: what is the gain? A nationwide survey. **Pediatrics** **121**:e416–e420, 2008

---

Manuscript submitted January 6, 2010.

Accepted April 1, 2010.

Portions of this work were presented in poster form at the 50th Experimental Nuclear Magnetic Resonance Conference, Pacific Grove, California, March 29–April 3, 2009.

Portions of this work were presented as an oral presentation at the 38th Annual Meeting of the AANS/CNS Section on Pediatric Neurological Surgery, Boston, Massachusetts, December 2, 2009.

Address correspondence to: Steven J. Schiff, M.D., Ph.D., 212 Earth-Engineering Sciences Building, University Park, Pennsylvania 16802. email: sschiff@psu.edu.